Materials Today Communications 35 (2023) 105843

Contents lists available at ScienceDirect

Materials Today Communications

journal homepage: www.elsevier.com/locate/mtcomm

Effect of ultrafine microstructure on interdiffusion-driven phase transformations in Ni-Sn sandwich diffusion couples

N.K. Chaitanya, B. Yadav, P.P. Bhattacharjee, M. Vaidya *

Department of Materials Science and Metallurgical Engineering, Indian Institute of Technology Hyderabad, Kandi, Sangareddy 502285, Telangana, India

ARTICLE INFO

Keywords:
Ultrafine microstructure
Interdiffusion
Diffusion couple
Phase growth
Microscopy

ABSTRACT

Solid-state diffusion in materials is greatly influenced by microstructural features such as grain boundaries, dislocations, and second phase particles. However, a systematic investigation of structure-kinetics correlation during interdiffusion is largely missing. Herein, a novel sandwich diffusion couple approach was utilized to demonstrate the effects of microstructure on interdiffusion-driven phase formation in the Ni-Sn system. Pure Ni samples were prepared by cold rolling (CR) and spark plasma sintering (SPS) with different microstructures. Two sandwich diffusion couples were prepared– a) Ni^{AM}/Sn/Ni^{CR} and b) Ni^{CR}/Sn/Ni^{SPS}, for phase growth analysis at each interface after annealing at 200 °C for 96 h. The intermetallic phase Ni_3Sn_4 formed at the Ni^{AM}/Sn, Ni^{CR}/Sn, and Ni^{SPS}/Sn interfaces had the thickness of 6, 14, and 41 μm, respectively, consistent with larger parabolic growth constant for the Ni^{SPS}/Sn interfaces. The enhanced kinetics at the SPS interface could be attributed to the presence of ultrafine-grained (UFG) (~320 nm) microstructure dominated by high-angle boundaries.

1. Introduction

Advanced materials development demands the consistent tailoring of microstructures by thermomechanical processing, to achieve enhanced mechanical properties[1]. The microstructural development is also significantly affected by the atomic transport or diffusion process in materials [2] In addition to temperature, diffusion is greatly influenced by microstructural elements including grain boundaries (GBs), dislocations, and second phase particles. Lattice and grain boundaries (GBs) are the two most important paths of atomic transport in solids, the latter usually possessing a high diffusivity [3]. The nature and number of GBs in polycrystalline solids therefore affects the diffusivity of the material. This becomes particularly significant in ultra-fine-grained (UFG) materials, where the GB fraction is considerably large. For example, diffusion measurements conducted on ultrafine-grained (UFG) pure Cu and Cu-based alloys prepared by equal channel angular pressing (ECAP) revealed the existence of ultra-fast diffusion paths [4–7]. Enhanced GB diffusion has been shown in severely deformed Ni processed by equi channel angular pressing [8]. Belkacemi et al. [9] have demonstrated the presence of kinetically different GBs by correlative analysis using secondary ion mass spectrometry and a radiotracer approach. The appreciable difference in diffusivities alters the kinetics of diffusion-controlled processes in these UFG materials. For e.g., Fe-Cr alloy processed by high pressure torsion exhibits enhanced oxidation resistance due to the accelerated formation of Cr_2O_3 passive layer [10]. A significantly enhanced diffusivity along the moving recrystallization front has been demonstrated for UFG Ni [11]. Activation energies of grain growth are significantly lower in CoCrFeMnNi alloys processed by SPS (d ~ 180 nm) than CoCrFeMnNi produced by liquid melting route (d ~ 20 μm) [12].

A large portion of the diffusion literature deals with the atomic transport in single crystalline and CG materials. The kinetic measurements in UFG materials have been sporadic and limited to using radiotracer approach. The influence of type and number of GBs during interdiffusion has not been detailed in the reported literature. Interdiffusion between metals and alloys is frequently encountered in engineering components and devices, which is often an assembly of different types of materials, for e.g. in flip-chip technology [13], bond coating [14], production of Nb_3Sn superconductors[15], nano tubes and laminate structures [16]. The development of interdiffusion zone (IDZ) is expected to be altered with the change in microstructure of one or both the end members, which can affect the interface properties in relevant applications. This has motivated us to carry out systematic investigations of ultrafine microstructure on interdiffusion-driven phase transformations.

A novel use of sandwich diffusion couple methodology is proposed,

* Corresponding author.
E-mail address: vaidyam@msme.iith.ac.in (M. Vaidya).

https://doi.org/10.1016/j.mtcomm.2023.105843
Received 5 March 2023; Accepted 16 March 2023
Available online 23 March 2023

where a low melting metal is sandwiched between the CG and UFG samples of a high melting point (T_m) metal/alloy. This is schematically presented in Fig. 1. The use of low melting point metal would ensure development of reasonable width of IDZ even at low temperatures, while the use of high melting material in CG and UFG states would guarantee absence of grain growth during annealing. Since the entire set-up is annealed together in a fixture, identical heat treatment conditions are ensured minimizing any experimental uncertainties.

In the present study, pure Ni ($T_m = 1450$ °C) and pure Sn ($T_m = 232$ °C) are chosen as high melting and low melting materials, respectively. Interdiffusion of Sn and transition metals (TMs) play an important role in electronic applications and has been widely studied. For e.g. Ni is used as a diffusion barrier layer in flip-chip packaging to prevent the interaction of Cu interconnects and Sn (which comes from the solder), via the formation of the Ni_3Sn_4 intermetallic phase [17]. Z. Chen et al. [18] demonstrated the formation of Ni3Sn4 is preceded by appearance of an amorphous layer if special Ni microcone structures are used instead of electroplated Ni in Ni/Sn diffusion couples. The insertion of amorphous Co-W barrier layer has proven to be effective to prevent interdiffusion between Cu and Sn[19]. The number of intermetallic phases in interdiffusion zone of Au/Sn system decreases with decrease in temperature due to kinetic constraints [20]. A systematic influence of UFG structure on the growth behaviour of Ni/Sn diffusion couples, as studied in present work, can provide deeper insights in understanding the role of GBs on interdiffusion driven phase transformations. For a complete investigation, three types of Ni samples are chosen, for the sandwich diffusion couple, produced by arc melting (AM), cold rolling (CR) and spark plasma sintering (SPS).

2. Materials and methods

In this study, pure Ni samples have been prepared by arc melting (AM), cold rolling (CR), and spark plasma sintering (SPS), which resulted in varied microstructures. High-purity Ni and Sn pieces were arc melted under a controlled Ar atmosphere. The arc melted (AM) Ni as a 20×7x7 mm rectangular bar was multi-pass cold-rolled (CR) to 80% thickness reduction using laboratory rolling equipment (SPX precision equipment, Fenn division, USA). Alongside, High-purity Ni powder was ball milled for 10 h (h) followed by spark plasma sintering (SPS) (SCM 1050; Sumitomo Coal Mining Co, Ltd Japan) at 850 °C. CR-Ni and SPS-Ni specimens were annealed in an Ar atmosphere at 200 °C for 168 h to ensure the thermal stability of the microstructures during diffusion experiments. A reaction layer was sandwiched between the two end members of the same material having different microstructures (Fig. 1), and the assembly was subjected to diffusion annealing. The use of such a setup ensured that comparisons were made under identical conditions and reliable correlations were obtained. Two sandwich diffusion couples namely a) $Ni^{AM}/Sn/Ni^{CR}$ and b) $Ni^{AM}/Sn/Ni^{SPS}$, were prepared and annealed at 200 °C for 96 h for phase growth analysis at each of the interfaces.

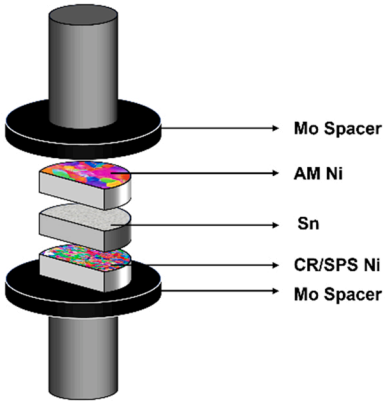

Fig. 1. Schematic of the sandwich diffusion couple methodology.

Prior to interdiffusion annealing, the $Ni^{AM}/Sn/Ni^{CR}$ and $Ni^{AM}/Sn/Ni^{SPS}$ sandwich diffusion couples were hot compacted at optimized conditions to ensure initial uniform bonding all over the interfaces. As depicted in Fig. 1, the sandwich diffusion couple was placed between the molybdenum foils to avoid diffusion with the stainless fixture, and the setup was annealed at 200° C for 96 h in an Ar atmosphere using a SiC furnace with a temperature accuracy of ± 1°. The microstructure of the as-processed and annealed samples, and the phases developed in the interdiffusion zones (IDZs) were analyzed using scanning electron microscopy (SEM) (JEOL-JSM 7800 F), electron probe microanalysis (EPMA) (JEOL JXA-8530 F) and electron backscattered diffraction (EBSD) (EDX-AMETEK Inc., USA).

3. Results and discussion

3.1. Microstructure of as-processed samples

The differences in the microstructure of AM, CR, and SPS Ni are highlighted in the EBSD IPF maps (Fig. 2((a)-(c)) and corresponding misorientation angle distribution plots (Fig. 2((d)-(f)). The Ni^{AM} shows a coarse-grained (CG) structure (grain size, $d \sim 200$ μm) with high angle boundaries (HABs) fraction of ~0.145 (Fig. 2a, d). Fig. 2b illustrates that Ni^{CR} develops a typical elongated morphology with grain width i.e. HAB spacing along the ND ~5 μm. The predominance of low angle boundaries (LABs) in Ni^{CR} is reflected in the misorientation distribution plot in Fig. 2e. An ultra-fine grained (UFG), nearly equiaxed microstructure with d ~ 320 nm is obtained in Ni^{SPS} (Fig. 2c). The UFG microstructure is consistent with a significantly high fraction of HABs (Fig. 2f). The unindexed pixels in the Ni^{SPS} (Fig. 2c) are due to the presence of residual porosity (< 8%).

Since the microstructures of end members must remain thermally stable during the diffusion annealing, Ni^{CR} and Ni^{SPS} samples have been pre-annealed at 200 °C for 168 h before the diffusion experiments. The microstructures of the pre-annealed Ni^{CR} and Ni^{SPS} samples are displayed in IPF maps (Fig. 3(a,b)). The misorientation angle distribution plot of pre-annealed Ni^{CR} in Fig. 3c manifest the dominance of low angle grain boundaries analogous to Ni^{CR} in fig2e. The grain size and the fraction of HAB in the pre-annealed Ni^{SPS} sample (Fig. 3(b,d)) matches with the Ni^{SPS} (Fig. 2(c,f)). Therefore, the EBSD analysis negates microstructural evolution or grain growth during this heat treatment.

3.2. Phase formation in the $Ni^{AM}/Sn/Ni^{CR}$ and $Ni^{AM}/Sn/Ni^{SPS}$ sandwich diffusion couples

Fig. 4a) and b) show the BSE micrographs and the corresponding composition profiles of the IDZs in the $Ni^{AM}/Sn/Ni^{CR}$ and $Ni^{AM}/Sn/Ni^{SPS}$ sandwich diffusion couples annealed for 200 °C/96 h. The compositional contrast indicates the evolution of a single phase across both interfaces. Several EDS line scans at both the interdiffusion zones (IDZs) have been carried out and the compositions obtained are as follows: 56–59 at% and 41–44 at% of Sn and Ni, respectively; thus confirming the formation of a Ni_3Sn_4 intermetallic phase.

The formation of Ni_3Sn_4 at the interface of Ni/Sn diffusion couples has also been observed in the literature [21,22]. In the Ni-Sn binary phase diagram, three intermetallic phases are observed at 200 °C, namely, Ni_3Sn, Ni_3Sn_2, and Ni_3Sn_4 [23]. However, at each of the interfaces in our studied diffusion couples, only Ni_3Sn_4 is obtained. This remarkable difference can be attributed to the fact that the diffusion annealing temperature (200 °C) corresponds to a significantly larger homologous temperature for Sn (0.9 T_m, T_m is the melting point) than for Ni (0.3 T_m). This implies that Sn diffusivity is much higher compared to Ni, and hence results in the preferential evolution of the Sn-rich Ni_3Sn_4 phase.

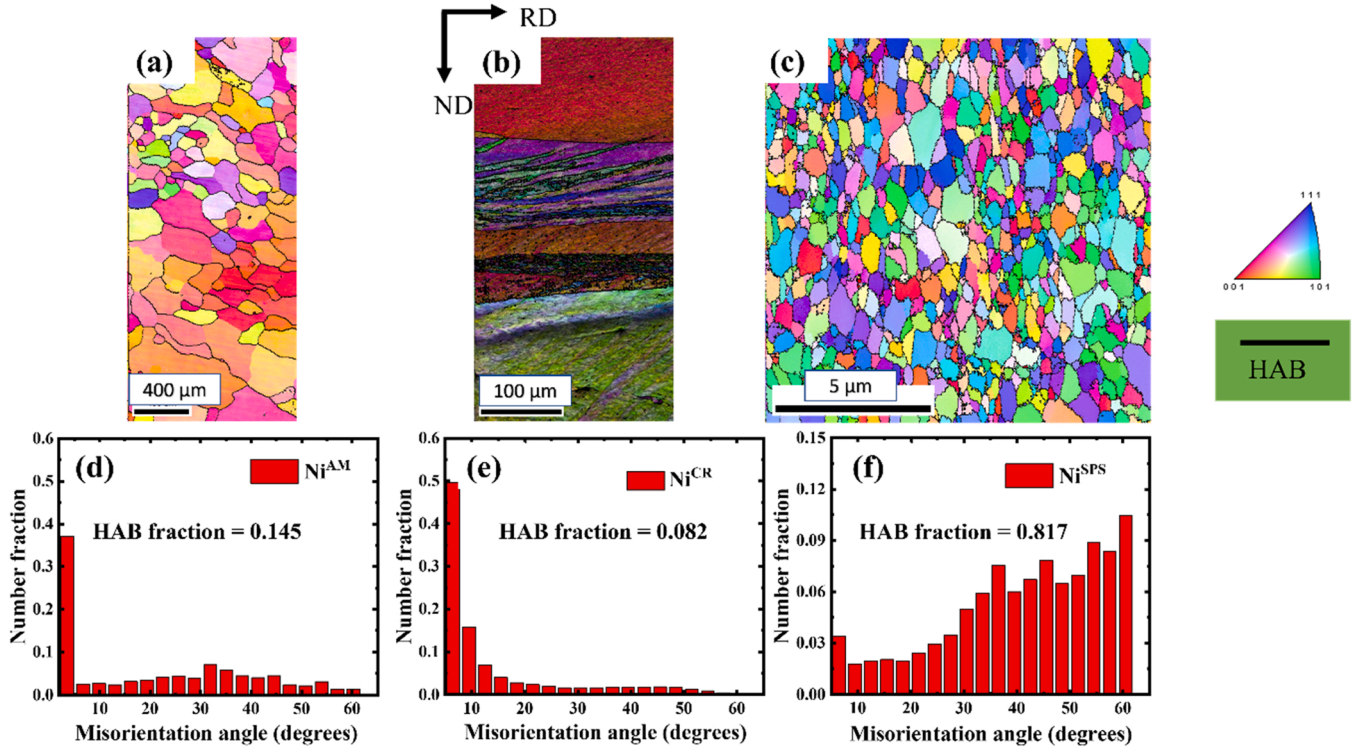

Fig. 2. EBSD ((a)-(c)) IPF maps and ((d)-(e)) the misorientation angle distribution plots of ((a),(d)) Ni^{AM}, ((b),(e)) Ni^{CR} and ((c),(f)) Ni^{SPS} (RD: rolling direction; TD: transverse direction).

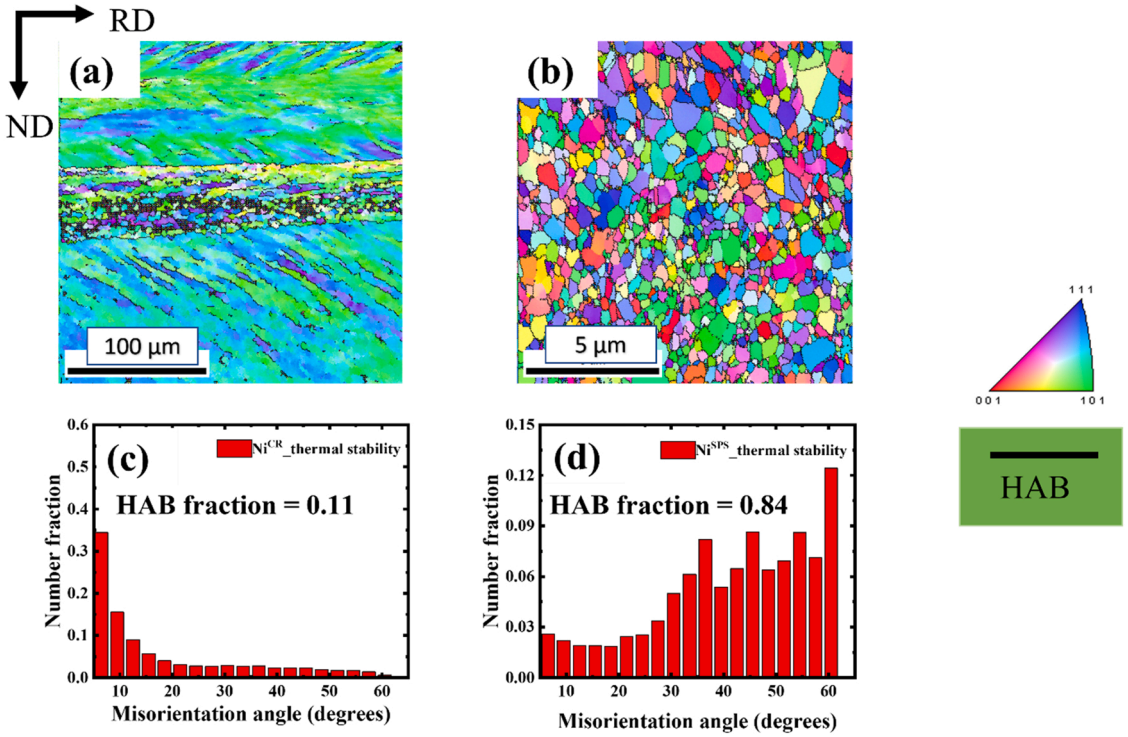

Fig. 3. EBSD ((a), (b)) IPF maps and ((c), (d)) the misorientation angle distribution plots of (a) Ni^{CR}_200°C,168 h and (b) Ni^{SPS} _200°C,168 h (RD: rolling direction; TD: transverse direction).

3.3. Kinetics of Ni_3Sn_4 phase growth

The kinetics of Ni_3Sn_4 growth have been shown to follow a parabolic growth law in the literature for Ni/Sn diffusion couples [21,22]. To confirm the nature of phase growth for Ni^{CR}/Sn, additional diffusion annealing for time intervals of 144, 192, and 216 h have also been carried out for Ni^{AM}/Sn/ Ni^{CR}. The evolution of the Ni_3Sn_4 phase with time at the Ni^{CR}/Sn interface is presented by plotting the variation of the

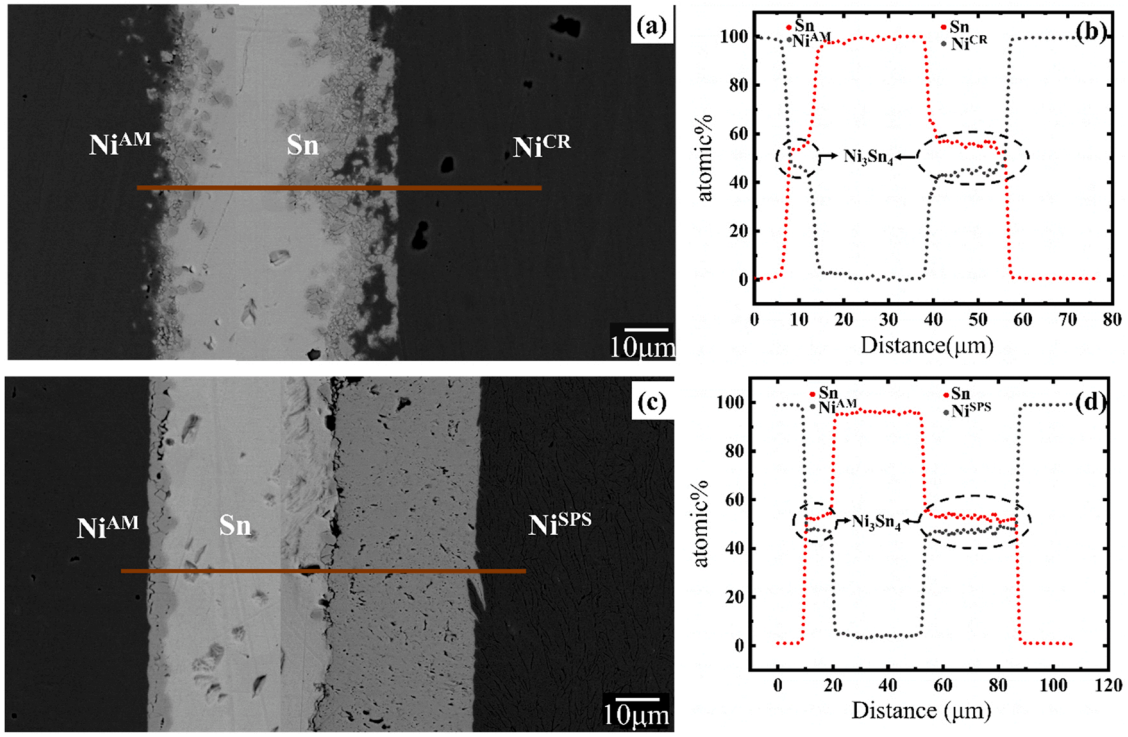

Fig. 4. ((a), (c)) BSE micrographs and the ((b), (d)) composition profiles of the ((a),(b)) Ni^{AM}/Sn/ Ni^{CR}, ((c),(d)) Ni^{AM}/Sn/ Ni^{SPS} sandwich diffusion couples, annealed for 200 °C/96 h.

square of the average thickness (Δx^2) with time (t) (Fig. 5a), which confirms a parabolic growth. The value of the parabolic growth constant (k_p) is estimated from the slope of the plot as 5.1×10^{-17} m^2/s.

The value of k_p for the growth of Ni_3Sn_4 at different interfaces in the present work and with the reported literature is compared in Fig. 5(b). The k_p at the AM-Ni/Sn interface is the least and agrees well with the literature values [21,22] reported for the case of coarse-grained Ni used in Ni/Sn interdiffusion. For the Ni^{CR} interface, a slight increase in k_p value is observed, which can be attributed to the generation of LABs during cold rolling. Such an increase in diffusivities has also been observed by Divinski et al. [24] for the cold-rolled Ni, when analyzed through the radiotracer approach. The k_p value at the Ni^{SPS}/Sn interface is significantly higher than that estimated for the Ni^{AM}/Sn and Ni^{CR}/Sn diffusion couples. This can be understood in terms of the considerably reduced grain size (~320 nm) of Ni^{SPS}, which implies a considerably high GB fraction. It is well established that the GBs offer a high-diffusivity path [25] in solids when compared to the lattice. A large GB area in Ni^{SPS}, therefore, leads to the increase in overall diffusion flux and hence faster growth of the intermetallic phase.

4. Conclusion

Two sandwich diffusion couples– a) Ni^{AM}/Sn/Ni^{CR} and b) Ni^{AM}/Sn/ Ni^{SPS} were prepared and annealed at 200 °C for 96 h. The formation of Ni_3Sn_4 phase was confirmed at each interface. The parabolic growth constant (k_p) is estimated at each of the interfaces. A slight increase in the k_p value was observed at the Ni^{CR}/Sn interface due to the LABs created during the deformation. A significant increase in the k_p value for Ni^{SPS} /Sn diffusion couple was observed, which was consistent with the UFG structure, high HAB fraction, and enhanced diffusion flux. Thus, the novel use of sandwich diffusion couple methodology to investigate structure-kinetics correlation during interdiffusion-driven phase

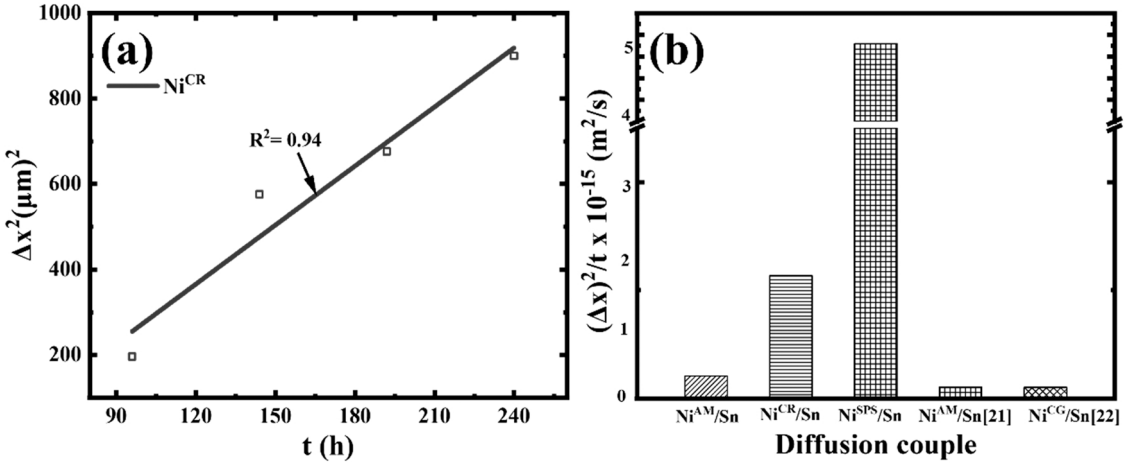

Fig. 5. a) phase growth kinetics of Ni_3Sn_4 phase at the Ni^{CR}/Sn interface b) $(\Delta x)^2/t$ vs Ni_3Sn_4 at different interfaces annealed at 200 °C, 96 h.

transformations was demonstrated in the present work.

CRediT authorship contribution statement

N. K. Chaitanya: Conceptualization, Methodology, Investigation, Writing – original draft, **Bhawna Yadav:** Investigation, Methodology, **P. P. Bhattacharjee**: Conceptualization, Methodology, Writing – original draft, Supervision, **Mayur Vaidya:** Conceptualization, Methodology, Writing – original draft, Supervision, Funding acquisition.

Declaration of Competing Interest

The authors declare that they have no known competing financial interests or personal relationships that could have appeared to influence the work reported in this paper.

Data Availability

Data will be made available on request.

Acknowledgments

The authors gratefully acknowledge the financial support of DST - SERB (Project No: SRG/2020/002172) and IIT Hyderabad Seed Grant for carrying out the research work.

References

[1] J. Zhao, Z. Jiang, Thermomechanical processing of advanced high strength steels, Prog. Mater. Sci. 94 (2018) 174–242, https://doi.org/10.1016/j.pmatsci.2018.01.006.
[2] T. Gietzelt, V. Toth, A. Huell, Challenges of diffusion bonding of different classes of stainless steels, Adv. Eng. Mater. 20 (2) (2018), 1700367, https://doi.org/10.1002/adem.201700367.
[3] H. Masuda, E. Sato, Diffusional and dislocation accommodation mechanisms in superplastic materials, Acta Mater. 197 (2020) 235–252, https://doi.org/10.1016/j.actamat.2020.07.042.
[4] Y. Amouyal, S.V. Divinski, L. Klinger, E. Rabkin, Grain boundary diffusion and recrystallization in ultrafine grain copper produced by equal channel angular pressing, Acta Mater. 56 (19) (2008) 5500–5513, https://doi.org/10.1016/j.actamat.2008.07.029.
[5] J. Ribbe, G. Schmitz, Y. Amouyal, Y. Estrin, S.V. Divinski, Grain boundary radiotracer diffusion of ni in ultra-fine grained Cu and Cu - 1wt% Pb alloy produced by equal channel angular pressing, Mater. Sci. Forum 584-586 (2008) 380–386, https://doi.org/10.4028/www.scientific.net/MSF.584-586.380.
[6] S. Divinski, G. Wilde, E. Rabkin, Y. Estrin, Ultra-fast atomic transport in severely deformed materials-a pathway to applications? Adv. Eng. Mater. 12 (8) (2010) 779–785, https://doi.org/10.1002/adem.200900340.
[7] P.B. Straumal, M. Wegner, D.V. Shangina, O.A. Kogtenkova, A. Kilmametov, S. V. Divinski, S.V. Dobatkin, G. Wilde, Diffusion of 63Ni in severely deformed ultrafine grained Cu-based alloys, Scr. Mater. 127 (2017) 141–145, https://doi.org/10.1016/j.scriptamat.2016.07.008.
[8] E. Osinnikov, S. Murzinova, A.Y. Istomina, V. Popov, A. Stolbovskiy, R. Falahutdinov, Grain-boundary diffusion of 57 Co in ultrafine nickel after severe plastic deformation, Phys. Met. Metallogr. 122 (2021) 976–980, https://doi.org/10.1134/S0031918×21100082.
[9] L. Belkacemi, M. Vaidya, S. Sevlikar, A. Hassanpour, F. Jomard, D. Irmer, C. Guerre, L. Martinelli, C. Duhamel, G. Wilde, Intrinsic heterogeneity of grain boundary states in ultrafine-grained Ni: a cross-scale study by SIMS and radiotracer analyses, Materialia 22 (2022), 101397, https://doi.org/10.1016/j.mtla.2022.101397.
[10] K. Ding, E. Bruder, C. Dietz, K. Durst, X. Fang, Nanoindentation study of the oxide scale on FeCr alloy by high-pressure torsion, Corros. Sci. 194 (2022), 109951, https://doi.org/10.1016/j.corsci.2021.109951.
[11] D. Prokoshkina, L. Klinger, A. Moros, G. Wilde, E. Rabkin, S.V. Divinski, Effect of recrystallization on diffusion in ultrafine-grained Ni, Acta Mater. 69 (2014) 314–325, https://doi.org/10.1016/j.actamat.2014.02.002.
[12] M. Vaidya, A. Anupam, J.V. Bharadwaj, C. Srivastava, B. Murty, Grain growth kinetics in CoCrFeNi and CoCrFeMnNi high entropy alloys processed by spark plasma sintering, J. Alloy. Compd. 791 (2019) 1114–1121, https://doi.org/10.1016/j.jallcom.2019.03.341.
[13] B. Kim, Y. Sohn, Analysis of intermetallic compound formation in the reactions at liquid Ga/solid Pd interface, Surf. Interfaces 30 (2022), 101951, https://doi.org/10.1016/j.surfin.2022.101951.
[14] S. Dong, Y. Li, M. Xu, S. Li, Z. Dong, Z. Bao, S. Zhu, F. Wang, Effect of Re-base diffusion barrier on the oxidation performance of a gradient NiCoCrAlY coating, Surf. Coat. Technol. 452 (2023), 129105, https://doi.org/10.1016/j.corsci.2021.109919.
[15] D. Sharma, D. Kalyan, S.K. Makineni, S. Santra, Effect of Zr on growth kinetics, microstructure and microtexture of Nb3Sn by bronze technique, J. Alloy. Compd. 935 (2023), 168140, https://doi.org/10.1016/j.jallcom.2022.168140.
[16] H.-K. Kang, Y.-S. Kang, D.-K. Kim, M. Baik, J.-D. Song, Y. An, H. Kim, M.-H. Cho, Al2O3 passivation effect in HfO2·Al2O3 laminate structures grown on InP substrates, ACS Appl. Mater. Interfaces 9 (20) (2017) 17526–17535, https://doi.org/10.1021/acsami.7b00099.
[17] T. Huang, S. Liu, H. Ling, M. Li, A. Hu, L. Gao, T. Hang, Growth behavior and morphology of sidewall intermetallic compounds in Cu/Ni/sn-Ag microbumps during multiple reflows, Mater. Lett. 326 (2022), 132887, https://doi.org/10.1016/j.matlet.2022.132887.
[18] Z. Chen, M. Cai, Z. Liu, Y. Chen, X. Yi, F. Wang, W. Zhu, Amorphization and intermetallic nucleation in early-stage interfacial diffusion during Sn-solder/Ni solid-state bonding, J. Alloy. Compd. 859 (2021), 158399, https://doi.org/10.1016/j.jallcom.2020.158399.
[19] S. Chen, L. Tan, C. Yang, P. Chen, A. Hu, H. Ling, M. Li, T. Hang, Effects of amorphous CoW and NiW barrier layers on the evolution of Sn/Cu interface, Mater. Charact. 181 (2021), 111448, https://doi.org/10.1016/j.matchar.2021.111448.
[20] V.A. Baheti, S. Kashyap, P. Kumar, K. Chattopadhyay, A. Paul, Solid–state diffusion–controlled growth of the phases in the Au–Sn system, Philos. Mag. 98 (1) (2018) 20–36, https://doi.org/10.1080/14786435.2017.1392052.
[21] V.A. Baheti, S. Kashyap, P. Kumar, K. Chattopadhyay, A. Paul, Solid–state diffusion–controlled growth of the intermediate phases from room temperature to an elevated temperature in the Cu–Sn and the Ni–Sn systems, J. Alloy. Compd. 727 (2017) 832–840, https://doi.org/10.1016/j.jallcom.2017.08.178.
[22] M. Mita, M. Kajihara, N. Kurokawa, K. Sakamoto, Growth behavior of Ni3Sn4 layer during reactive diffusion between Ni and Sn at solid-state temperatures, Mater. Sci. Eng.: A 403 (1–2) (2005) 269–275, https://doi.org/10.1016/j.msea.2005.05.012.
[23] Alloy Phase diagrams, ASM International 1992.
[24] M. Shepelenko, L. Klinger, E. Rabkin, A. Berner, D. Prokoshkina, G. Reglitz, J. Fiebig, G. Wilde, S.V. Divinski, Recovery, recrystallization and diffusion in cold-rolled Ni, Int. J. Mater. Res. 106 (6) (2015) 554–564, https://doi.org/10.3139/146.111217.
[25] T.L.A. Paul, V. Vuorinen, S.V. Divinski, Thermodynamics, Diffusion and the Kirkendall Effect in Solids, Springer, 2014, https://doi.org/10.1007/978-3-319-07461-0.